Available online at www.sciencedirect.com
SCIENCE DIRECT®
ELSEVIER
International Journal of Solids and Structures 41 (2004) 6129–6146
INTERNATIONAL JOURNAL OF SOLIDS and STRUCTURES
www.elsevier.com/locate/ijsolstr

A small-scale magnetic-yielding model for an infinite magnetostrictive plane with a crack-like flaw

Y.P. Wan [a], D.N. Fang [a,*], A.K. Soh [b]

[a] Department of Engineering Mechanics, Tsinghua University, Beijing 100084, PR China
[b] Department of Mechanical Engineering, University of Hong Kong, Hong Kong, PR China

Received 27 April 2004; accepted 1 May 2004
Available online 10 June 2004

Abstract

The effect of an external magnetic field on the fracture toughness of magnetostrictive materials has been investigated by determining the local stress fields around the tip of a very slender elliptical flaw embedded in an infinite magnetostrictive plane subjected to magnetic loading, based on the assumption of linear magnetization. In this paper, the above-mentioned analytical approach is extended to develop a small-scale magnetic-yielding model. The magnetic saturation zone is constructed and the distributions of magnetic field and magnetization are obtained around the tip of a slender elliptical crack. Based on the complex potential theory, the stress field is obtained in the vicinity of the tip of the slender elliptical crack by implementing the continuity conditions of displacement and resultant force at the interface between the magnetic saturation and magnetoelastic zones. The stress fields near the tip of the slender elliptical crack are obtained for two kinds of soft ferromagnetic materials each with a small induction magnetostrictive modulus. The theoretical results obtained show that the stresses in the neighborhood of a crack-tip are finite even when the elliptical crack reduces to a sharp crack, and are much smaller than the yield stress or the nominal fracture stress of the material. This suggests that, generally, the magnetic field has no obvious effects on the apparent fracture toughness of soft ferromagnetic materials, which is in agreement with the existing experimental results published in the existing literature. In addition, the theoretical analysis illustrates that no crack is magnetically impermeable, and the corresponding boundary conditions are inappropriate for fracture analysis of soft ferromagnetic materials.

Keywords: Magnetostrictive material; Small-scale magnetic-yielding; Fracture toughness; Elliptical crack

1. Introduction

The soft ferromagnetic materials (SFMs) have been widely used in engineering. More and more researchers have paid attention to the mechanical properties of the SFMs subjected to external magnetic fields (Moon and Pao, 1968; Pao and Yeh, 1973; Van De Ven, 1978; Zhou and Zheng, 1996; Yang et al.,

* Corresponding author. Tel./fax: +86-10-62772923.
E-mail address: fangdn@mail.tsinghua.edu.cn (D.N. Fang).

0020-7683/$ - see front matter © 2004 Elsevier Ltd. All rights reserved.
doi:10.1016/j.ijsolstr.2004.05.008

1999; Zhou and Miya, 1999). The effect of magnetic field on the apparent toughness of SFMs has been investigated by some researchers using theoretical (Shindo, 1977, 1978, 1982, 1983, 1985; ANG, 1989; Shindo and Horiguchi, 1991; Sabir and Maugin, 1996; Bagdasarian and Hasanian, 2000) and experimental techniques (Clatterbuck et al., 2000; Wan et al., 2003b). In the past two decades, the manufacturing capability of giant magnetostrictive materials has been greatly improved. Many kinds of giant magnetostrictive compounds consisting of rare earth elements have been fabricated with high quality and at relatively low cost, which makes it feasible for engineering application of magnetostrictive materials. The distinct superiority of the magnetostrictive materials over the ordinary ferromagnets is their significant magnetostriction (Clark, 1980). Therefore, it is a known fact that the non-linear deformation and fracture induced by magnetostriction should be properly accounted for in the study of magnetostrictive materials subjected to external magnetic-mechanical loading. In the previous work of the authors (Wan, 2002; Wan et al., 2003c), linear magnetization and isotropic constitutive relations for magnetostrictive materials were adopted to investigate the deformation and fracture behavior of infinite soft ferromagnetic solids with an elliptical crack. The magnetic body force and the magnetic traction induced by surface magnetization were taken into account. For several kinds of specific soft ferromagnetic materials, the effect of a magnetic field on the apparent fracture toughness was analyzed.

Under a low magnetic field, the magneto-strain varies linearly with the square of magnetic field. When the external magnetic field is very high, the strain induced by the magnetostrictive effect is likely to saturate (Clark, 1980; Wan et al., 2003a). For a soft magnetostrictive material with a crack-like flaw subjected to an external magnetic field, saturation of magnetization tends to occur near the tip of the crack-like flaw due to the concentration of magnetic field. Thus, in this paper, an attempt is made to determine the stress field around the tip of a crack-like flaw by adopting a model of perfect magnetization saturation based on the analysis presented in Wan et al. (2003c), in which linear magnetization was a prerequisite, and small deformation prevails and the assumption that deformation exerts negligibly small disturbance to the distribution of magnetic field is adopted. In the present study, we also specify the case where electric current is absent and the external magnetic field is quasi-static. The magnetization saturation zone is assumed to be a cylinder. By using the continuity conditions of displacement and resultant force along the interface between the saturation and linear magnetization zones, the stress solution is obtained based on the classical complex potential method (Muskhelishvili, 1963). This method has been successfully employed to determine the stress fields around the edge of an electric pole in the electrostrictive material with a cylindrical region of perfect polarization saturation (Hao et al., 1996). However, when the problem of crack-like flaw is studied, it should be noted that the intensity of the magnetic field varies with the change of the width of the crack-like flaw (i.e., the concentration of magnetic field increases as the slender elliptical flaw reduces to a sharp crack). Thus, the size and location of the saturation zone would be changed. Furthermore, the boundary conditions of the crack surface must be taken into consideration to obtain the final stress fields inside the saturation zone.

2. The magnetization saturation zone

Many soft ferromagnetic materials, for example, the soft ferromagnetic steels and the series of manganese–zinc ferrites, are generally susceptible to magnetization under magnetic field. These materials have large magnetostriction and very small energy loss due to the narrow hysteresis loops. The constitutive law can be approximated as isotropic, apparent magnetostrictive and history-independent due to very small energy loss (refer to Fig. 1). Under an external magnetic field, a ferromagnetic crystal exhibits length variation, both in the direction of the magnetic field (i.e., longitudinal direction) and perpendicular to it (i.e., transverse direction). This is termed as magnetostriction. The magneto-strain of SFMs is related to the magnitude of magnetic field. Generally, the strain is a quadratic function of the magnetic field when the

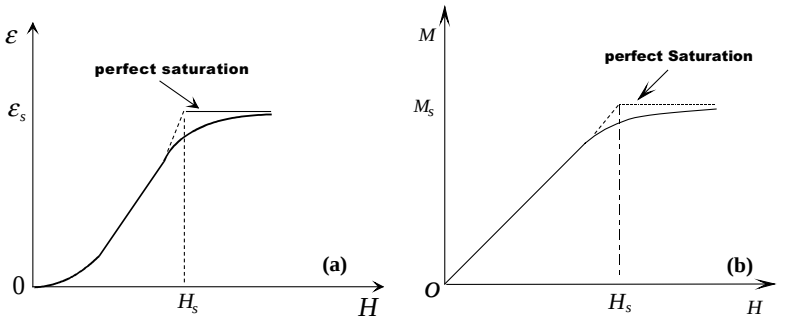

Fig. 1. The perfect saturation model: (a) magnetostrictive curve and (b) magnetization curve.

magnetic field is not very strong. In this case the standard square model for the constitutive relation is valid (Wan et al., 2003a). When the external magnetic field becomes very intense (refer to Fig. 1(a)), the magneto-strain approaches the saturation point, ε_s, which is generally deemed as a material constant. Fig. 1(b) shows the magnetization curve of a typical soft ferromagnetic material, where H_s refers to the magnetic field at which magnetization of the material is saturated, and M_s is the corresponding saturated magnetization. When the magnetic field is not very strong, the magnetization increases almost linearly with increasing external magnetic field. As the magnetic field becomes very intense, the magnetization reaches a saturation point, M_s, which is also a material constant.

In the present study, the external magnetic field is assumed to be smaller than H_s, but the magnetic field near the crack-tip may be higher than H_s due to the concentration effect. Therefore, the material is still linearly magnetic, except for a small volume around the tip of the elliptical crack. This is so-called the small-scale magnetic-yielding condition. For simplicity, a reasonable assumption of perfect saturation of magnetization (refer to the dashed lines in Fig. 1) is made in the present study. This is to say the major part of the material is linearly magnetized with respect to the magnetic field that is lower than the saturation point. Based on the above-mentioned assumption, the material has a constant magneto-strain, ε_s, in the small region around the tip of the slender elliptical crack.

In the linearly magnetized region, the distribution of the magnetic field in the neighborhood of the crack-tip has been obtained by Wan et al. (2003c) as follows:

$$H_1 = -\frac{K_H}{\sqrt{2\pi r}} \sin\frac{\theta}{2}, \tag{1a}$$

$$H_2 = \frac{K_H}{\sqrt{2\pi r}} \cos\frac{\theta}{2}, \tag{1b}$$

where H_1 and H_2 are the x and y components of the magnetic field vector, respectively (refer to Fig. 2); and K_H is the magnetic intensity factor. The magnitude of the magnetic field vector is

$$H = \sqrt{(H_1)^2 + (H_2)^2}. \tag{2}$$

This distribution is approximately valid in a hollow cylinder whose inner radius is that of the saturated cylinder, and whose outer radius is much smaller than the crack length (refer to Fig. 2). The characteristic length, r_s, can be obtained by letting $H = H_s$, i.e.,

$$r_s = \frac{1}{2\pi}\left(\frac{K_H}{H_s}\right)^2. \tag{3}$$

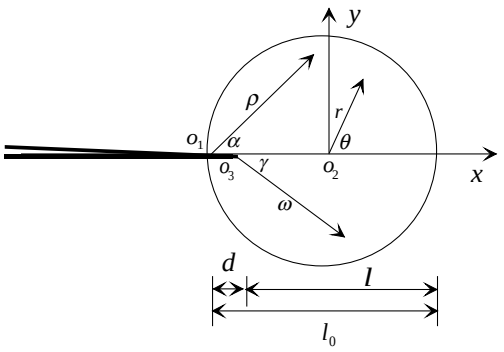

Fig. 2. The size and position of the magnetization saturation zone.

Since the magnetic flux can neither be stopped nor disappear in the magnetic material, the segment length of the saturation zone ahead of the crack-tip can be estimated by means of the following expression:

$$l_0 = \frac{1}{M_s}\int_0^{r_s} (\mu_1 H)\,\mathrm{d}r, \tag{4}$$

where $M_s = \chi_1 H_s$ is the saturation magnetization of the material, χ_1 is the susceptibility of the material; μ_1 is the permeability of the material; and r is the distance away from the crack-tip along the crack face. The length of the saturation segment, l_0, can be easily estimated as $l_0 = 2r_s$. For the slender elliptical crack whose minor semi-axis is not zero, i.e., $b \neq 0$, the magnetic field at the tip of a slender elliptical crack must be bounded. The distribution of the magnetic field along the major axis has been predicted by Wan et al. (2003c) as follows:

$$H = \frac{1}{2}\frac{a(1+\Delta_1)}{\sqrt{2ar+b^2}}H^{\infty}, \tag{5}$$

where r is the distance away from the tip and along the major semi-axis of the slender elliptical crack, H^{∞} is the remotely applied magnetic field and Δ_1 can be expressed as

$$\Delta_1 = \frac{\frac{b}{a}\frac{\mu_1}{\mu_2} - 1}{\frac{b}{a}\frac{\mu_1}{\mu_2} + 1}, \tag{6}$$

where μ_1 and μ_2 are the permeability of the materials outside and inside the slender elliptical crack, respectively; b and a are the minor and major semi-axes of the elliptical crack, respectively. The magnetic field intensity factor can be expressed as

$$K_H = \frac{1}{2}(1+\Delta_1)\sqrt{\pi a}H^{\infty}. \tag{7}$$

Thus, Eq. (5) becomes

$$H = K_H\sqrt{\frac{a}{\pi}}\frac{1}{\sqrt{2ar+b^2}}. \tag{8}$$

In terms of Eq. (8), the estimated length of the saturation segment along the major axis of the slender crack is given by (refer to Fig. 2):

$$l = \sqrt{(2r_s)^2 + \frac{2r_s}{a}b^2} - \sqrt{\frac{2r_s}{a}}b. \tag{9}$$

The length of the saturation segment behind the tip (denoted as d) can be obtained by letting $d = l_0 - l$. Generally, soft ferromagnetic materials have a large permeability. When the medium inside the crack is air or vacuum, $\mu_1 \gg \mu_2$. Thus, the following condition generally prevails for a slender elliptical crack:

$$\frac{H^\infty/H_s}{b/a + \mu_2/\mu_1} \gg 1. \tag{10a}$$

Based on Eqs. (3) and (7), Eq. (10a) can be rewritten as

$$\frac{b}{\sqrt{2ar_s}} \ll 1. \tag{10b}$$

Hence, the expressions of d and l are reduced to

$$d = b\sqrt{\frac{2r_s}{a}}, \tag{11a}$$

$$l = 2r_s - b\sqrt{\frac{2r_s}{a}}. \tag{11b}$$

It can be verified that $d \ll l$ for a slender elliptical flaw where $b \to 0$ but $b \neq 0$. Only when the slender elliptical flaw reduces to a sharp crack, i.e., $b = 0$, then $d = 0$. For a general case where the minor axis of the elliptical flaw is not equal to zero, i.e., $b \neq 0$, $d > 0$, which implies that the saturation cylinder must intersect the slender elliptical crack at two symmetrical points (refer to Fig. 3).

3. The magnetic field and magnetization in the saturation zone

With the assumption of linear magnetization, the distribution of the magnetic field near the tip of a slender elliptical crack (Wan et al., 2003c) is as follows:

$$H_r = \frac{K_H}{\sqrt{2\pi r}}\sin\frac{\theta}{2}, \tag{12a}$$

$$H_\theta = \frac{K_H}{\sqrt{2\pi r}}\cos\frac{\theta}{2}, \tag{12b}$$

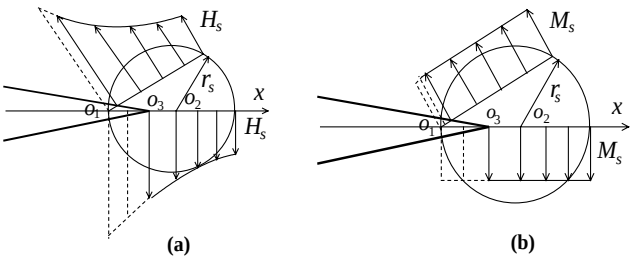

Fig. 3. The distribution of the magnetic field (a) and magnetization in the saturation zone (b).

where r, θ are the polar coordinates with origin o_2 (refer to Fig. 2). The corresponding potential function of this magnetic field is given by

$$\Phi = -K_H\sqrt{\frac{2r}{\pi}}\sin\frac{\theta}{2}. \tag{13}$$

At the interface between the cylindrical saturation region and the outside magnetoelastic area, where $r = r_s$ and $\theta = 2\alpha$, in which α is the polar angle of the polar coordinates with origin o_1 (refer to Fig. 2), the magnetic potential becomes

$$\Phi = -K_H\sqrt{\frac{2r_s}{\pi}}\sin\alpha. \tag{14}$$

The general relations between the magnetic field and its scalar potential can be expressed as

$$H_\rho = -\frac{\partial\Phi}{\partial\rho}, \tag{15a}$$

$$H_\alpha = -\frac{1}{\rho}\frac{\partial\Phi}{\partial\alpha}, \tag{15b}$$

where ρ, α are the polar coordinates centered at o_1 (refer to Fig. 2). The magnetic field inside the cylindrical saturation zone can be obtained by substituting Eq. (14) into Eqs. (15a) and (15b) as follows:

$$H_\rho = 0, \tag{16a}$$

$$H_\alpha = \frac{K_H}{\rho}\sqrt{\frac{2r_s}{\pi}}\cos\alpha. \tag{16b}$$

Obviously, the magnetic field becomes singular at point o_1 at which $\rho = 0$. As pointed out in Wan et al. (2003c), the magnetic field inside the elliptical crack is homogeneous and no singularity exists. Since point o_1 is located in the slender elliptical crack, singularity does not really exist. The intersecting points of the boundary of the cylindrical saturation zone and that of the elliptical crack can be analytically obtained through solving the simultaneous equations describing the said zone and crack. Since the saturation zone is symmetrical with respect to the x-coordinate, the upper portion can be selected as the representative part for simplicity. The polar angle of the intersecting point, α_0, is determined as follows:

$$\alpha_0 = \frac{1}{2}\arccos\frac{\frac{b}{a}(c + r_s) - \sqrt{b^2 + c^2 - a^2 + 2cr_s + \frac{a^2}{b^2}r_s^2}}{\left(\frac{a}{b} - \frac{b}{a}\right)r_s}. \tag{17}$$

Therefore, the saturated region can be expressed as $|\alpha| \leqslant \alpha_0$ in the coordinate system centered at o_1, where $|\alpha|$ represents the absolute value of the polar angle α. The magnetic field on the surface of the slender elliptical crack within the region, $|\alpha| \leqslant \alpha_0$, can be obtained as follows:

$$H_\alpha = K_H\sqrt{\frac{2r_s}{\pi}}\frac{\left(\frac{b^2}{a^2}\cos^2\alpha + \sin^2\alpha\right)\cos\alpha}{-c\frac{b^2}{a^2}\cos\alpha + \sqrt{b^2\left(\frac{b^2}{a^2}\cos^2\alpha + \sin^2\alpha\right) - c^2\frac{b^2}{a^2}\sin^2\alpha}}, \tag{18}$$

where $c = a - d$ (refer to Fig. 2). The polar component, H_ρ, of the magnetic field equals to zero. Therefore, the magnetic field along the surface of the slender elliptical crack is bounded. The direction of magnetization coincides with that of magnetic field, and its magnitude equals to M_s. Thus,

$$M_\rho = 0, \tag{19a}$$

$$M_\alpha = M_s, \tag{19b}$$

where M_s is saturation magnetization, which has been defined above. From the above formulae, it can be seen that the magnetic potential is continuous on the interface between the cylindrical saturation region and the outside area, and there is no jump of magnetic field across the interface. In accordance with the magnetic force theory developed by Brown Jr. (1966), there is no surface magnetization across the cylindrical region and no surface magnetic force exists as well.

4. The stress field around the tip of an elliptical crack

Generally speaking, the saturation magneto-strain, ε_s, for a soft ferromagnetic material is a constant, which can be taken as an eigenstrain induced by the magnetic field in the saturation zone. Since the cylindrical saturation zone can be considered as an inclusion with an eigenstrain, the stress field of this problem can be obtained by solving a linear elastic inclusion problem, plus a pure elastic problem with tractions acting on the surface of an elliptical crack.

4.1. The continuity conditions of the cylindrical saturation region

Similar to the approach adopted by Hao et al. (1996) to determine the electrostrictive stress field in a saturation cylinder around an electric edge, the stress field induced by the misfit strain due to perfect saturation inside the cylindrical zone can be obtained by using the complex potential method and implementing the continuity conditions of displacement and resultant force on the boundary of the cylindrical saturation region. The magnetization in the afore-mentioned region induces a stress-free deformation. The magneto-strains are given by

$$\varepsilon_\rho = (1+\nu)m_{21}M_s^2, \tag{20a}$$

$$\varepsilon_\alpha = (m_{11}+\nu m_{21})M_s^2, \tag{20b}$$

$$\varepsilon_{\rho\alpha} = 0. \tag{20c}$$

For the small deformation case, the geometric equations in the polar coordinates can be expressed as

$$\varepsilon_\rho = \frac{\partial u_\rho}{\partial \rho}, \tag{21a}$$

$$\varepsilon_\alpha = \frac{1}{\rho}\frac{\partial u_\alpha}{\partial \alpha} + \frac{u_\rho}{\rho}, \tag{21b}$$

$$\varepsilon_{\rho\alpha} = \frac{1}{2}\left(\frac{1}{\rho}\frac{\partial u_\rho}{\partial \alpha} + \frac{\partial u_\alpha}{\partial \rho} - \frac{u_\alpha}{\rho}\right). \tag{21c}$$

Obviously, the displacements can be obtained by integrating Eqs. (21a)–(21c). The displacements are transformed from polar to rectangular coordinates by

$$u_1 + u_2\mathrm{i} = \mathrm{e}^{\alpha\mathrm{i}}(u_\rho + u_\alpha\mathrm{i}), \tag{22}$$

where $\mathrm{i} = \sqrt{-1}$; u_1 and u_2 are the displacement components in the rectangular coordinates. Note that the rigid body displacements correspond to the stress-free and strain-free states and, therefore, can be discarded. Thus, the displacements on the interface between the cylindrical region and the outside area satisfy the following form:

$$2G(u_1 + \mathrm{i}u_2) = Gr_s(1 + \mathrm{e}^{\theta\cdot\mathrm{i}})[2\varepsilon_\rho + i(\varepsilon_\alpha - \varepsilon_\rho)\theta], \tag{23}$$

where G is the shear modulus of the material. Let ϕ_1 and ψ_1 represent the complex potentials of the induced stress field in the saturation zone; and ϕ_2, ψ_2 denote the potentials in the linear magnetization area. On the boundary of the cylindrical saturation zone, the continuity conditions of the displacements and resultant force are given by

$$\begin{aligned}&(3-4v)\phi_1 - t\overline{\phi_1'} - \overline{\psi_1} + Gr_s(1+\mathrm{e}^{\theta\mathrm{i}})[2\varepsilon_\rho + \mathrm{i}(\varepsilon_\alpha - \varepsilon_\rho)\theta]\\ &\quad = (3-4v)\phi_2 - t\overline{\phi_2'} - \overline{\psi_2} + \sqrt{2ar_s}\left(p_1\,\mathrm{e}^{\frac{\theta_i}{2}} + p_2\,\mathrm{e}^{\frac{-\theta_i}{2}} + p_3\,\mathrm{e}^{\frac{3\theta_i}{2}}\right) + p_4\,\mathrm{e}^{\theta\cdot\mathrm{i}} + p_5\theta\mathrm{i},\end{aligned} \tag{24a}$$

$$\phi_1 + t\overline{\phi_1'} + \overline{\psi_1} = \phi_2 + t\overline{\phi_2'} + \overline{\psi_2} + \sqrt{2ar_s}\left(q_1\,\mathrm{e}^{\frac{\theta_i}{2}} + q_2\,\mathrm{e}^{\frac{-\theta_i}{2}} + q_3\,\mathrm{e}^{\frac{3\theta_i}{2}}\right) + q_4\,\mathrm{e}^{\theta\cdot\mathrm{i}} + q_5, \tag{24b}$$

where $t = r_s\,\mathrm{e}^{\theta\cdot\mathrm{i}}$ is a point on the cylindrical boundary. The coefficients, p_i ($i = 1$–5) and q_i ($i = 1$–5), are given in Appendix A. The jump conditions of the complex potentials across the cylindrical boundary can be derived from Eqs. (24a) and (24b), i.e.,

$$\phi_1 - \phi_2 = D_1\theta\mathrm{i} + D_2\,\mathrm{e}^{\theta\cdot\mathrm{i}} + D_3\theta\,\mathrm{e}^{\theta\cdot\mathrm{i}}\mathrm{i} + D_4\,\mathrm{e}^{\frac{\theta}{2}\cdot\mathrm{i}} + D_5\,\mathrm{e}^{-\frac{\theta}{2}\cdot\mathrm{i}} + D_6\,\mathrm{e}^{\frac{3\theta}{2}\cdot\mathrm{i}} + D_7, \tag{25a}$$

$$\psi_1 - \psi_2 = A_1\theta\mathrm{i} + A_2\,\mathrm{e}^{-\frac{\theta_i}{2}} + A_3\,\mathrm{e}^{-\frac{3\theta_i}{2}} + A_4\,\mathrm{e}^{-\frac{5\theta_i}{2}} + A_5\,\mathrm{e}^{\frac{\theta_i}{2}} + A_6\,\mathrm{e}^{-\theta\cdot\mathrm{i}} + A_7\,\mathrm{e}^{-2\theta\cdot\mathrm{i}} + A_8\theta\,\mathrm{e}^{-\theta\cdot\mathrm{i}}\mathrm{i} + A_9, \tag{25b}$$

where the coefficients D_i ($i = 1$–7) and A_i ($i = 1$–9) are given in Appendix B. To separate the complex potentials from the jump conditions (25a) and (25b), the following three conditions should be satisfied (Hao et al., 1996): (1) the displacements and the resultant force are continuous across the cylindrical boundary; (2) $z = -r_s$ is a virtual singularity point, at which the magnetic field and the stresses, and therefore, the complex potentials, ϕ_1, ψ_1, are singular. Thus, ϕ_1, ψ_1 are analytic in the whole saturation zone except for $z = -r_s$; (3) there is no stress at infinity, which means that ϕ_2, ψ_2 vanish at infinity. The complex potentials in Eqs. (25a) and (25b) can be separated distinctively in terms of the above three conditions and can be further extended into the saturation zone and the linear magnetization region based on the method adopted by Hao et al. (1996). The complex potentials with respect to the coordinates centered at o_2 are given as follows:

$$\phi_1(z) = D_1\ln\frac{z+r_s}{r_s} + D_2\frac{z}{r_s} + D_3\frac{z}{r_s}\ln\frac{z+r_s}{r_s} + D_4\sqrt{\frac{z}{r_s}} + D_6\frac{z}{r_s}\sqrt{\frac{z}{r_s}} + D_7 - D_3, \tag{26a}$$

$$\phi_2(z) = -D_1\ln\frac{z}{z+r_s} - D_3\left(1 + \frac{z}{r_s}\ln\frac{z}{z+r_s}\right) - D_5\sqrt{\frac{r_s}{z}}, \tag{26b}$$

$$\psi_1(z) = A_1\ln\frac{z+r_s}{r_s} + A_5\sqrt{\frac{z}{r_s}} + A_9, \tag{26c}$$

$$\psi_2(z) = -A_1\ln\frac{z}{z+r_s} - \left[A_2\sqrt{\frac{r_s}{z}} + A_3\frac{r_s}{z}\sqrt{\frac{r_s}{z}} + A_4\left(\frac{r_s}{z}\right)^2\sqrt{\frac{r_s}{z}}\right] - A_6\frac{r_s}{z} - A_7\left(\frac{r_s}{z}\right)^2 - A_8\frac{r_s}{z}\ln\frac{z}{r_s}. \tag{26d}$$

The stress field can be estimated by means of the complex potentials for the saturation and the linear magnetization zones. In the neighborhood of the tip of the slender elliptical crack ($\omega \to 0$), $z = -r_s + d + \omega\,\mathrm{e}^{\gamma\mathrm{i}}$, and the stress fields are in the following form:

$$\frac{\sigma_{22} + \sigma_{11}}{2} = 2\mathrm{Re}\left[\frac{D_1}{d + \omega\,\mathrm{e}^{\gamma\mathrm{i}}} + \frac{D_3}{r_s}\left(\frac{d - r_s}{d + \omega\,\mathrm{e}^{\gamma\mathrm{i}}} + \ln\frac{d + \omega\,\mathrm{e}^{\gamma\mathrm{i}}}{r_s}\right)\right], \tag{27a}$$

$$\frac{\sigma_{22}-\sigma_{11}}{2}+\mathrm{i}\sigma_{12}=(d-r_{\mathrm{s}})\left[\frac{D_3-D_1}{(d+\omega\mathrm{e}^{\gamma\mathrm{i}})^2}+\frac{D_3}{r_{\mathrm{s}}}\frac{1}{d+\omega\mathrm{e}^{\gamma\mathrm{i}}}\right]+\frac{A_1}{d+\omega\mathrm{e}^{\gamma\mathrm{i}}}, \tag{27b}$$

where ω and γ are the polar radius and angle of the polar coordinates centered at o_3, respectively. Re( ) represents the real part of the complex. The hoop stress along the major axis ($\gamma=0$) ahead of the tip is

$$\sigma_{22}^{(1)}=\frac{A_1+2D_1-3D_3}{d+\omega}+3\frac{D_3}{r_{\mathrm{s}}}\frac{d}{d+\omega}+\frac{(r_{\mathrm{s}}-d)(D_1-D_3)}{(d+\omega)^2}+2\frac{D_3}{r_{\mathrm{s}}}\ln\frac{d+\omega}{r_{\mathrm{s}}}. \tag{28}$$

4.2. An elastic problem with tractions acting on the surface of the elliptical crack

In order to obtain the final solution of the stress field, the solution of a purely elastic problem should be added, by inverting the tractions on the surface of the elliptical crack, to that obtained in the above subsection. It is assumed that the two magnetization zones, which are located at the tips of the slender elliptical crack, do not interact with each other since the size of the magnetization zone is much smaller than the length of the major axis in the small-scale magnetic-yielding model. The tractions on the surface of the slender elliptical crack can be estimated using the stress field obtained in the above subsection. It can be verified that the stress field in the vicinity of the origin, o_1, derived using the complex potentials ϕ_1, ψ_1 is identical to that obtained using ϕ_2, ψ_2. By substituting the complex potentials ϕ_1, ψ_1 into the stress Eqs. (A.1) and (A.2) in Appendix A, the stress field in the neighborhood of the origin, o_1, can be obtained as follows:

$$(\sigma_{11})_1=-\frac{r_{\mathrm{s}}(D_1-D_3)}{\rho^2}\cos 2\alpha, \tag{29a}$$

$$(\sigma_{22})_1=\frac{r_{\mathrm{s}}(D_1-D_3)}{\rho^2}\cos 2\alpha, \tag{29b}$$

$$(\sigma_{12})_1=-\frac{r_{\mathrm{s}}(D_1-D_3)}{\rho^2}\sin 2\alpha, \tag{29c}$$

where ρ and α are the polar radius and angle of the coordinates centered at o_1, respectively. $(\sigma_{\alpha\beta})_1$ represent the stress components with respect to the coordinates centered at o_1, which can be transformed into that centered at o by (refer to Fig. 2)

$$x=x_1+c,\quad y=y_1, \tag{30}$$

where x and y are the rectangular coordinates centered at o, and x_1 and y_1 are those centered at o_1. The stress field in Eq. (29) can be expressed in terms of the coordinates with origin o

$$\sigma_{11}=-r_{\mathrm{s}}(D_1-D_3)\frac{(x-c)^2-y^2}{[(x-c)^2+y^2]^2}, \tag{31a}$$

$$\sigma_{22}=r_{\mathrm{s}}(D_1-D_3)\frac{(x-c)^2-y^2}{[(x-c)^2+y^2]^2}, \tag{31b}$$

$$\sigma_{12}=-r_{\mathrm{s}}(D_1-D_3)\frac{2(x-c)y}{[(x-c)^2+y^2]^2}. \tag{31c}$$

The tractions acting on the inner surface of the slender elliptical crack (the side with its outward normal pointing into the ellipse) are

$$X = -(n_x)_1(\sigma_{11})_1 - (n_y)_1(\sigma_{12})_1, \tag{32a}$$

$$Y = -(n_x)_1(\sigma_{12})_1 - (n_y)_1(\sigma_{22})_1, \tag{32b}$$

where X and Y are the traction components along the ellipse. $(n_\alpha)_1$ represents the components of the unit outward normal of the ellipse with respect to the coordinate system with origin o_1. The stress field near the elliptical crack can be obtained by employing the classical method of complex potential (Muskhelishvili, 1963). In order to employ the formula provided in Muskhelishvili (1963), the tractions in Eq. (32) are further transformed to the coordinate system with origin o (refer to Fig. 2). Since the exerted tractions are of the same magnitude as those in Eq. (32) but in opposite direction, in the coordinate system with origin o, the exerted tractions acting on the inner surface of the ellipse are

$$X = n_x\sigma_{11} + n_y\sigma_{12}, \tag{33a}$$

$$Y = n_x\sigma_{12} + n_y\sigma_{22}, \tag{33b}$$

where n_α represents the components of the unit outward normal of the ellipse in the coordinate system centered at o; $\sigma_{\alpha\beta}$ are the stress components in the same coordinate system. In accordance with the complex potential theory (Muskhelishvili, 1963), the following equation can be written:

$$f = \int (X + \mathrm{i}Y)\,\mathrm{d}s. \tag{34}$$

By using the components, $n_x = \mathrm{d}y/\mathrm{d}s$, $n_y = -\mathrm{d}x/\mathrm{d}s$, where $\mathrm{d}s$ is an infinitesimal arc, the tractions can be expressed as

$$f = \int [\sigma_{11}\,\mathrm{d}y - \sigma_{12}\,\mathrm{d}x + \mathrm{i}(\sigma_{12}\,\mathrm{d}y - \sigma_{22}\,\mathrm{d}x)]. \tag{35}$$

Substituting Eqs. (31a)–(31c) into Eq. (35) renders

$$f = r_s(D_1 - D_3)\int \frac{[(x-c)^2 - y^2](-\mathrm{i}\,\mathrm{d}x - \mathrm{d}y) + [2(x-c)y](\mathrm{d}x - \mathrm{i}\,\mathrm{d}y)}{[(x-c)^2 + y^2]^2}. \tag{36}$$

By using $x = \frac{1}{2}(z + \bar{z})$, $y = \frac{1}{2i}(z - \bar{z})$ and performing integration, Eq. (36) becomes

$$f = \mathrm{i}\left[\frac{r_s(D_1 - D_3)}{\bar{z} - c} - C_0\right], \tag{37}$$

where C_0 is a constant that depends on the starting point of the integration contour. It can be seen that the function in Eq. (37) is single-valued and analytic, which implies that integration of the tractions along a contour equals zero, and hence, the resultant traction vanishes on a closed integration contour. Note that the tractions are self-balanced. The classical complex potential theory (Muskhelishvili, 1963) can be applied to an infinite plane elastic problem with an elliptical crack, where a self-balanced traction is exerted on the elliptical surface and no mechanical loads are applied at infinity. The conformal mapping function, $z = w(\zeta)$, is selected such that the domain in the physical plane outside the elliptical flaw is mapped into the area outside the unit circle of the mapping plane, i.e.,

$$z = w(\zeta) = R(\zeta + m\zeta^{-1}), \tag{38}$$

where z, and ζ are the complex variables in the physical plane and the mapping plane, respectively, and $R = (a+b)/2,\ m = (a-b)/(a+b),\ z = x+iy,\ \zeta = \xi + i\eta$. The complex potentials are obtained in the physical plane (ζ) as follows:

$$\phi(\zeta) = 0, \tag{39a}$$

$$\psi(\zeta) = \frac{-r_s(D_1 - D_3)}{R(\alpha_1 - \alpha_2)}\left(\frac{\alpha_1}{\alpha_1 - \zeta} - \frac{\alpha_2}{\alpha_2 - \zeta}\right), \tag{39b}$$

in which

$$\alpha_1 = \frac{a - d + \mathrm{i}\sqrt{2ad - b^2 - d^2}}{a+b}, \tag{40a}$$

$$\alpha_2 = \frac{a - d - \mathrm{i}\sqrt{2ad - b^2 - d^2}}{a+b}, \tag{40b}$$

where $\mathrm{i} = \sqrt{-1}$. The stresses are obtained from Eqs. (A.1) and (A.2) in Appendix A

$$\sigma_{22} + \sigma_{11} = 0, \tag{41a}$$

$$\sigma_{22} - \sigma_{11} + 2\mathrm{i}\sigma_{12} = -\frac{2r_s(D_1 - D_3)}{R^2}\frac{\zeta^2}{\left[\alpha_1\alpha_2 - (\alpha_1 + \alpha_2)\zeta + \zeta^2\right]^2}. \tag{41b}$$

With the inverse mapping function

$$\zeta = \frac{z + \sqrt{z^2 - a^2 + b^2}}{a+b}, \tag{42}$$

the stresses in Eqs. (41a) and (41b) can be re-expressed in the physical plane. By substituting $z = a + \omega$ into Eq. (42), and then into Eq. (41), the hoop stress on the crack line immediately ahead of the tip of the slender elliptical crack ($\omega \to 0$) is obtained, i.e.,

$$\sigma_{22}^{(2)} = -r_s(D_1 - D_3)/(d+\omega)^2. \tag{43}$$

5. Examples and discussions

The final hoop stress on the crack extension line inside the saturation zone is the sum of Eqs. (28) and (43), that is $\sigma_{22} = \sigma_{22}^{(1)} + \sigma_{22}^{(2)}$. Thus, we obtain

$$\sigma_{22} = \frac{A_1 + 2D_1 - 3D_3}{d+\omega} + 3\frac{D_3}{r_s}\frac{d}{d+\omega} - \frac{d(D_1 - D_3)}{(d+\omega)^2} + 2\frac{D_3}{r_s}\ln\frac{d+\omega}{r_s}, \tag{44}$$

in which d, D_1, D_3 and A_1 are given in Eqs. (11a), (B.1), (B.3) and (B.8), respectively; and ω is the distance away from the tip of the slender elliptical crack (refer to Fig. 2). The final hoop stress outside the saturation zone, which is given in Appendix C, can be obtained through performing similar calculations. The calculations consist of three parts, i.e., the stress obtained from the potentials given in Eqs. (26b) and (26d), the stress given in Eq. (43), and that of linear magnetization already given in Wan et al. (2003c).

The medium inside the slender elliptical crack is generally assumed to be air or vacuum. Thus, $\mu_2/\mu_1 = 1/\mu_r$, where μ_r is the relative permeability of the material. To the best of the authors' knowledge, there are only two existing fracture experiments on the soft ferromagnetic materials with a small induction magnetostrictive modulus, i.e., the soft ferromagnetic alloy steel (Clatterbuck et al., 2000), and the

manganese–zinc ferrite (Wan et al., 2003b). In this section, the theoretical model of small-scale magnetic saturation is used to account for the experimental results for these two soft ferromagnetic materials.

(1) Fig. 4 shows the plots of the hoop stress on the crack extension line for these two soft ferromagnetic materials, in which the symbols $h1$, $h2$ and $h3$ are defined as follows:

$$h1 = H^{\infty}/H_s, \quad h2 = b/a, \quad h3 = \mu_2/\mu_1. \tag{45}$$

It can be seen that the hoop stress on the crack extension line jumps across the interface between the cylindrical saturation zone and the outside area. The hoop stress at the tip can be obtained by letting $\omega = 0$ in Eq. (44), i.e.,

$$\sigma_{22} = \frac{A_1 + D_1 - 2D_3}{d} + \frac{D_3}{r_s}\left(3 - 2\ln\frac{r_s}{d}\right), \tag{46}$$

where r_s, d, D_1, D_3 and A_1 are given in Eqs. (3), (11a), (B.1), (B.3) and (B.8), respectively. It is obvious from Eq. (6) that Δ_1 gradually reduces to -1 and the saturation zone shrinks to the crack-tip when the slender elliptical crack becomes a sharp crack, i.e., $b = 0$. Fig. 5 presents the plots of the hoop stress at the tip against the ratio b/a for these two soft ferromagnetic materials. It can be seen that the hoop stress remains finite even when the elliptical crack becomes a sharp crack (i.e., b reduces to zero).

(2) One kind of soft ferromagnetic steel (Incoloy 908) had been employed to investigate the effect of external magnetic field on the apparent fracture toughness (Clatterbuck et al., 2000). The results showed that the applied magnetic field did not have any measurable effect on the fracture toughness of the ferromagnetic steel if experimental errors were taken into account. This phenomenon is evidently in agreement with the present theoretical result, which shows that the hoop stresses of 0.03 MPa and 0.05 MPa at the tip of the elliptical crack due to the external magnetic fields of $0.5H_s$ and $0.8H_s$, respectively, are negligible as compared with the yield stress (1191 MPa) and the ultimate strength (1454 MPa) of the ferromagnetic steel. By performing three-point-bending tests for the single-edge-beam specimens (Wan et al., 2003b), the authors had previously measured the fracture toughness of the manganese–zinc ferrite ceramic subjected to magnetic-mechanical loading. With the known fracture loading and the specimen geometry, the nominal maximum stress of the three-point bending is estimated to be 34 MPa by using the theory of beam bending for small deformation. It can be seen that the hoop stress at the tip of the slender elliptical crack (See Table 1) is far smaller than the nominal fracture stress. This clearly indicates that the effect of the external magnetic field on the apparent fracture toughness of the manganese–zinc ferrite ceramics is quite small and can be neglected.

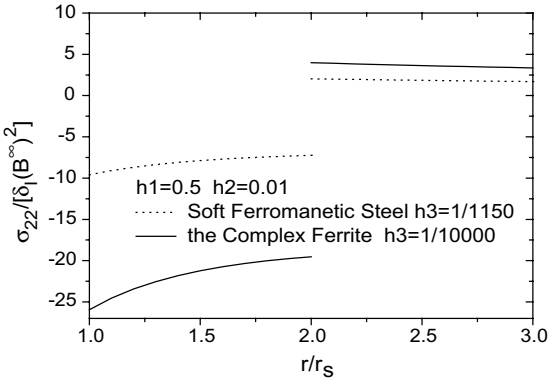

Fig. 4. Plots of the hoop stress on the segment directly ahead of the tip along the elliptical crack surface when the crack is vacuum ($\mu_2 = \mu_0$).

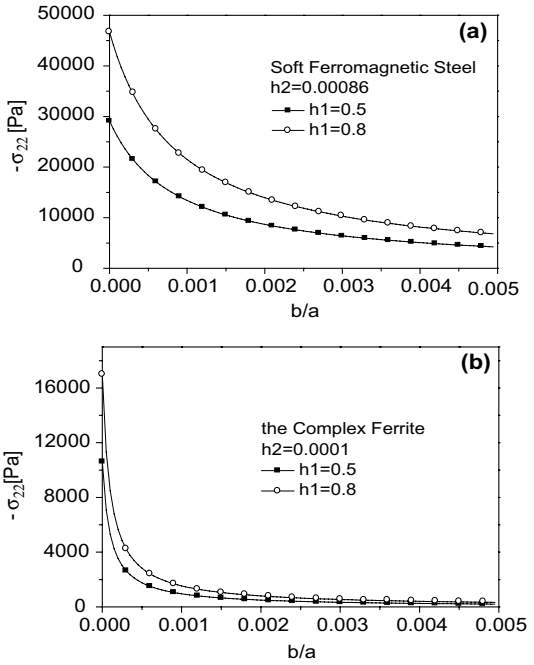

Fig. 5. The hoop stress at the tip of the slender elliptical crack when the medium inside the ellipse is air or vacuum. (a) A soft ferromagnetic alloy steel and (b) the manganese–zinc ferrite ceramics.

Table 1
The hoop stress at the tip of the slender elliptical crack

Geometry of the slender elliptical crack b/a	Hoop stress at the tip of the slender elliptical crack σ_{22} (MPa)		
	$\mu_r = 2000$	$\mu_r = 5000$	$\mu_r = 10,000$
0	−0.459	−0.318	−0.175
0.1	-19.2×10^{-5}	-69.85×10^{-5}	-252.7×10^{-5}

(3) The hoop stress in Eq. (44) reduces to Eq. (47) for a slit crack ($b = 0$) if the impermeable model is adopted, i.e., the permeability of the medium is taken to be zero inside the slender elliptical crack ($\mu_2 \equiv 0$)

$$\sigma_{22} = \frac{A_1 + 2D_1 - 3D_3}{\omega} + 2\frac{D_3}{r_s}\ln\frac{\omega}{r_s}, \tag{47}$$

where ω is the distance away from the crack-tip. Obviously, there is a singularity of ω^{-1} for the hoop stress on the crack extension line. For a central finite crack (Tada et al., 1985), the stress intensity factor (SIF) can be defined by $K = \lim_{\omega\to 0}\sqrt{2\pi\omega}\sigma_{22}$. The SIF for the impermeable model can be obtained as follows:

$$K = \lim_{\omega\to 0}\frac{\sqrt{2\pi}(A_1 + 2D_1 - 3D_3)}{\sqrt{\omega}}. \tag{48}$$

The SIF approaches infinity for a sharp crack, which obviously contradicts with the experimental results. Therefore, the impermeable model exaggerates the magnetoelastic effects of the magnetic field on soft ferromagnetic materials and produces results that do not agree with experimental data.

6. Conclusions

In this paper, a small-scale magnetic-yielding model is developed to determine the stress fields near the tip of a slender elliptical crack for soft ferromagnetic materials. The magnetic saturation zone is constructed and the distribution of the magnetic field is estimated. By using the complex potential theory, the hoop stress is obtained for two soft ferromagnetic materials, which are the soft ferromagnetic steel and the manganese–zinc ferrite ceramics. The following conclusions can be drawn from the analysis and comparison of the theoretical and experimental results:

(1) The hoop stress jumps across the interface of the saturation zone and the linear magnetization area. The stress remains finite at the tip even when the slender elliptical crack is reduced to a slit crack.
(2) For the soft ferromagnetic materials with a small induction magnetostrictive modulus, such as the soft ferromagnetic steel and the complex ferrite, the hoop stress obtained using the single-edge-notch-beam specimen is negligibly small compared to the yield stress of the steel or the nominal fracture stress of the complex ferrite ceramics. This analysis accounts for the non-obvious effect of magnetic field on the apparent fracture toughness of the soft ferromagnetic materials.
(3) The impermeable boundary conditions are inappropriate for fracture analysis of soft ferromagnetic materials. This boundary condition should not be adopted in the theoretical model, i.e., the permeability should not be taken as zero even if the inside of the slender elliptical crack is vacuum.

Acknowledgements

Support from the National Science Foundation of China under Grants #10025209, #10132010, #10102007 and from the Research Grants Council of the Hong Kong Special Administrative Region, China (Project No. HKU 7063/01E) is acknowledged.

Appendix A

In the complex potential theory, the displacements and resultant forces in an isotropic, linearly elastic solid can be represented by two analytic functions $\phi(z)$ and $\psi(z)$, where $z = re^{i\theta}$, $i = \sqrt{-1}$. The stresses, displacements and resultant forces can be expressed as follows:

$$\frac{\sigma_{22} + \sigma_{11}}{2} = \phi'(z) + \overline{\phi'(z)}, \tag{A.1}$$

$$\frac{\sigma_{22} - \sigma_{11}}{2} + i\sigma_{12} = \bar{z}\phi''(z) + \psi'(z), \tag{A.2}$$

$$2G(u_1 + iu_2) = (3 - 4v)\phi(z) - z\overline{\phi'(z)} - \overline{\psi(z)}, \tag{A.3}$$

$$F_1 + iF_2 = -i\left[\phi(z) + z\overline{\phi'(z)} + \overline{\psi(z)}\right], \tag{A.4}$$

where $(\,)'$ represents the derivative with respect to the complex variable, z; and $\overline{(\,)}$ denotes the complex conjugate. In the linear magnetization problem (Wan et al., 2003c), the basic governing equations and the associated boundary condition are:

$$\sigma_{\gamma\alpha,\gamma} + \delta_I \cdot (B_\gamma B_\gamma)_{,\alpha} = 0, \tag{A.5}$$

$$\varepsilon_{\alpha\beta} = \frac{1+v}{E}(\sigma_{\alpha\beta} - v\sigma_{\gamma\gamma}\delta_{\alpha\beta}) + (m_{11} - m21)B_\alpha B_\beta + (1+v)m_{21}B_\gamma B_\gamma \delta_{\alpha\beta}, \tag{A.6}$$

$$\varepsilon_{\alpha\beta} = \frac{1}{2}(u_{\alpha,\beta} + u_{\beta,\alpha}), \tag{A.7}$$

where α, β and γ run from 1 to 2. B_α are the components of the magnetic induction vector, and $B_\alpha = \mu_0\mu_r H_\alpha$; μ_0 is the permeability of the vacuum and μ_r the relative permeability of material. E and v are Young's modulus and Poisson's ratio, respectively. m_{11} and m_{21} are designated as the induction magnetostrictive modulus of the matrix material (Wan et al., 2003a). $(*)_{,\alpha}$ denotes the derivative of $(*)$ with respect to the Cartesian coordinates, x_α. The stresses at infinity must be zero and the boundary condition along the elliptical contour is

$$n_\beta\sigma_{\alpha\beta} = n_\alpha[\delta_{\mathrm{II}}(B_\gamma B_\gamma)_{\mathrm{II}} - \delta_{\mathrm{I}}(B_\gamma B_\gamma)_{\mathrm{I}}] \tag{A.8}$$

and

$$\delta_\alpha = \frac{\chi_\alpha}{\mu_0(1+\chi_\alpha)^2}(\alpha = \mathrm{I}, \mathrm{II}), \tag{A.9}$$

where χ is the magnetic susceptibility. The subscripts I and II denote the matrix outside the ellipse and the medium in the elliptical flaw, respectively. The displacements and resultant forces on the circle are as follows:

$$2G(u_1 + \mathrm{i}u_2) = \sqrt{2ar_s}\left(p_1 \mathrm{e}^{\frac{\theta_i}{2}} + p_2 \mathrm{e}^{-\frac{\theta_i}{2}} + p_3 \mathrm{e}^{\frac{3\theta_i}{2}}\right) + p_4 \mathrm{e}^{\theta_i} + p_5\theta\mathrm{i}, \tag{A.10}$$

$$F_1 + \mathrm{i}F_2 = -\mathrm{i}\left[\sqrt{2ar_s}\left(q_1 \mathrm{e}^{\frac{\theta_i}{2}} + q_2 \mathrm{e}^{-\frac{\theta_i}{2}} + q_3 \mathrm{e}^{\frac{3\theta_i}{2}}\right) + q_4 \mathrm{e}^{\theta\cdot\mathrm{i}} + q_5\right], \tag{A.11}$$

in which the coefficients are as follows:

$$p_1 = \left[\frac{3-4v}{2}(\beta + \kappa\Delta_1) + \frac{\kappa}{4}(1-\Delta_1^2)\right](\mu_1 H^\infty)^2, \tag{A.12}$$

$$p_2 = \left[-\frac{1}{4}(\beta + \kappa\Delta_1) + \frac{\kappa}{8}(1-\Delta_1^2) + \frac{G}{2}(m_{11} - m_{21})(1-\Delta_1^2)\right](\mu_1 H^\infty)^2, \tag{A.13}$$

$$p_3 = \left[-\frac{1}{4}(\beta + \kappa\Delta_1) + \frac{\kappa}{8}(1-\Delta_1^2)\right](\mu_1 H^\infty)^2, \tag{A.14}$$

$$p_4 = \frac{\kappa}{4}(1+\Delta_1)^2 a(\mu_1 H^\infty)^2, \tag{A.15}$$

$$p_5 = -\frac{G}{8}(m_{11} - m_{21})(1+\Delta_1)^2 a(\mu_1 H^\infty)^2, \tag{A.16}$$

$$q_1 = \left[\frac{1}{2}(\beta + \kappa\Delta_1) - \frac{\beta}{4}(1-\Delta_1^2)\right](\mu_1 H^\infty)^2, \tag{A.17}$$

$$q_2 = \left[\frac{1}{4}(\beta + \kappa\Delta_1) - \frac{\kappa}{8}(1-\Delta_1^2)\right](\mu_1 H^\infty)^2, \tag{A.18}$$

$$q_3 = \left[\frac{1}{4}(\beta + \kappa\Delta_1) - \frac{\beta}{12}(1-\Delta_1^2) - \frac{\kappa}{24}(1-\Delta_1^2)\right](\mu_1 H^\infty)^2, \tag{A.19}$$

$$q_4 = -\frac{\beta+\kappa}{8}(1+\Delta_1)^2 a(\mu_1 H^\infty)^2, \tag{A.20}$$

$$q_5 = \sqrt{2ar_s}\left[-(\beta+\kappa\Delta_1)+\frac{\beta}{3}(1-\Delta_1^2)+\frac{\kappa}{6}(1-\Delta_1^2)\right](\mu_1 H^\infty)^2+\frac{\beta+\kappa}{8}(1+\Delta_1)^2 a(\mu_1 H^\infty)^2, \tag{A.21}$$

in which the constants and symbols are as follows:

$$\kappa = S - \frac{E'\delta_I}{4(\lambda+G)}, \tag{A.22}$$

$$S = \frac{1-(1+2v)q}{4}E' m_{11}, \tag{A.23}$$

$$E' = \frac{E}{1-v^2}, \quad q = -\frac{m_{21}}{m_{11}}, \quad \beta = \kappa + \delta_I, \tag{A.24}$$

$$\delta_I = \frac{\chi_I}{\mu_0(1+\chi_I)^2}, \tag{A.25}$$

χ_I is the magnetic susceptibility, E and v are Young's modulus and Poisson's ratio, respectively, m_{11} and m_{21} are designated as the induction magnetostrictive moduli of the material.

Appendix B

$$D_1 = \frac{p_5}{4(1-v)} - \frac{Gr_s}{4(1-v)}(\varepsilon_\alpha - \varepsilon_\rho), \tag{B.1}$$

$$D_2 = \frac{p_4+q_4}{4(1-v)} - 2\varepsilon_\rho\frac{Gr_s}{4(1-v)}, \tag{B.2}$$

$$D_3 = -\frac{Gr_s}{4(1-v)}(\varepsilon_\alpha - \varepsilon_\rho), \tag{B.3}$$

$$D_4 = \frac{p_1+q_1}{4(1-v)}\sqrt{2ar_s}, \tag{B.4}$$

$$D_5 = \frac{p_2+q_2}{4(1-v)}\sqrt{2ar_s}, \tag{B.5}$$

$$D_6 = \frac{p_3+q_3}{4(1-v)}\sqrt{2ar_s}, \tag{B.6}$$

$$D_7 = \frac{q_5}{4(1-v)} - 2\varepsilon_\rho\frac{Gr_s}{4(1-v)}, \tag{B.7}$$

$$A_1 = \frac{(3-2v)p_5}{4(1-v)} + \frac{(-3+2v)Gr_s}{4(1-v)}(\varepsilon_\alpha - \varepsilon_\rho), \tag{B.8}$$

$$A_2 = \sqrt{2ar_s}\left[\frac{(-3+2v)p_1}{4(1-v)} + \frac{(5-6v)q_1}{4(1-v)} - \frac{3(p_3+q_3)}{8(1-v)}\right], \tag{B.9}$$

$$A_3 = \sqrt{2ar_s}\left[\frac{(-3+2v)p_3}{4(1-v)} + \frac{(5-6v)q_3}{4(1-v)} - \frac{p_1+q_1}{8(1-v)}\right], \tag{B.10}$$

$$A_4 = \sqrt{2ar_s}\frac{p_2+q_2}{8(1-v)}, \tag{B.11}$$

$$A_5 = \sqrt{2ar_s}\left[\frac{(-3+2v)p_2}{4(1-v)} + \frac{(5-6v)q_2}{4(1-v)}\right], \tag{B.12}$$

$$A_6 = \frac{(-2+v)p_4}{2(1-v)} + \frac{(2-3v)q_4}{2(1-v)} + Gr_s\left[\frac{7-4v}{4(1-v)}\varepsilon_\rho + \frac{1}{4(1-v)}\varepsilon_\alpha\right], \tag{B.13}$$

$$A_7 = -\frac{p_5}{4(1-v)} + \frac{Gr_s}{4(1-v)}(\varepsilon_\alpha - \varepsilon_\rho), \tag{B.14}$$

$$A_8 = \frac{(-1+v)Gr_s}{2(1-v)}(\varepsilon_\alpha - \varepsilon_\rho), \tag{B.15}$$

$$A_9 = \frac{(5-6v)q_5}{4(1-v)} + \frac{(3-2v)Gr_s}{4(1-v)}2\varepsilon_\rho \tag{B.16}$$

Appendix C

The total hoop stress on the crack extension line outside the cylindrical saturation zone is

$$\sigma_{22} = \frac{-3D_3}{\omega+r_s} - \frac{(D_1+A_1)r_s}{\omega(\omega+r_s)} + r_s\frac{A_6-(D_1-D_3)}{\omega^2} + \frac{D_1r_s}{(\omega+r_s)^2} + \left(\frac{1}{2}A_2 + \frac{1}{4}D_5\right)\frac{\sqrt{r_s}}{\omega\sqrt{\omega}} - \frac{2D_3}{r_s} \times \ln\left(\frac{\omega}{\omega+r_s}\right) + \frac{D_3\omega}{(\omega+r_s)^2} - \frac{3}{2}A_3\frac{r_s\sqrt{r_s}}{\omega^2\sqrt{\omega}} + \frac{5}{2}A_4\frac{r_s^2\sqrt{r_s}}{\omega^3\sqrt{\omega}} + 2A_7\frac{r_s^2}{\omega^3} - A_8\frac{r_s^2}{\omega^3}\left[1-\ln\left(\frac{\omega}{r_s}\right)\right]. \tag{C.1}$$

References

ANG, W.T., 1989. Magnetic stresses in an anisotropic soft ferromagnetic material with a crack. International Journal of Engineering Science 27, 1519–1526.

Bagdasarian, G.Y., Hasanian, D.J., 2000. Magnetoelastic interaction between a soft ferromagnetic elastic half-plane with a crack and a constant magnetic field. International Journal of Solids and Structures 37, 5371–5383.

Brown Jr., W.F., 1966. Magnetoelastic Interactions. Springer, New York.

Clark, A.E., 1980. Magnetostrictive rare earth-Fe_2 compounds. Ferromagnetic materials. In: Wohlfarth, E.P., (Ed.), vol 1, North-Holland Publishing Company.

Clatterbuck, D.M., Chan, J.W., Morris Jr., J.W., 2000. The influence of a magnetic field on the fracture toughness of ferromagnetic steel. Materials Transactions, JIM 41, 888–892.

Hao, T.H., Gong, X., Suo, Z., 1996. Fracture mechanics for the design of ceramic multilayer actuators. Journal of the Mechanics and Physics of Solids 44, 23–48.

Moon, F.C., Pao, Y.H., 1968. Magnetoelastic buckling of a thin plate. ASME Journal of Applied Mechanics 35, 53–58.

Muskhelishvili, N.I., 1963. Some Basic Problems of the Mathematical Theory of Elasticity. Noordhoff, Netherlands.

Pao, Y.H., Yeh, C.S., 1973. A linear theory for soft ferromagnetic elastic solids. International Journal of Engineering Science 11, 415–436.

Sabir, M., Maugin, G.A., 1996. On the fracture of paramagnets and soft ferromagnets. International Journal of Non-linear Mechanics 31, 425–440.

Shindo, Y., 1977. The linear magnetoelastic problem for a soft ferromagnetic elastic solid with a finite crack. ASME Journal of Applied Mechanics 44, 47–50.

Shindo, Y., 1978. Magnetoelastic interaction of a soft ferromagnetic elastic solid with a penny-shaped crack in a constant axial magnetic field. ASME Journal of Applied Mechanics 45, 291–296.

Shindo, Y., 1982. The linear magnetoelastic problem of two coplanar griffith cracks in a soft ferromagnetic elastic strip. ASME Journal of Applied Mechanics 49, 69–74.

Shindo, Y., 1983. Dynamic singular stresses for a griffith crack in a soft ferromagnetic elastic solid subjected to a uniform magnetic field. ASME Journal of Applied Mechanics 50, 50–56.

Shindo, Y., 1985. Impact response of a cracked soft ferromagnetic medium. Acta Mechanica 57, 99–112.

Shindo, Y., Horiguchi, K., 1991. Dynamic bending of cracked soft ferromagnetic plate in uniform magnetic field. Theoretical and Applied Fracture Mechanics 15, 207–217.

Tada, H., Paris, P.C., Irwin, G.R., 1985. The Stress Analysis of Cracks Handbook. Del Research, St. Louis, MO.

Van De Ven, A.A.F., 1978. Magnetoelastic buckling of thin plates in a uniform transverse magnetic field. Journal of Elasticity 8, 297–312.

Wan, Y.P., 2002. Experimental and theoretical study on the constitutive relation and fracture behavior of the magnetostrictive materials, Ph.D. Dissertation, Department of Engineering Mechanics, Tsinghua University, Beijing.

Wan, Y.P., Fang, D.N., Hwang, K.C., 2003a. Nonlinear constitutive relations for magnetostrictive materials. International Journal of Non-linear Mechanics 38, 1053–1065.

Wan, Y.P., Fang, D.N., Soh, A.K., 2003b. Effects of magnetic field on fracture toughness of manganese–zinc ferrite ceramics. Modern Physics Letters B 17, 57–66.

Wan, Y.P., Fang, D.N., Soh, A.K., Hwang, K.C., 2003c. Effect of magnetostriction on fracture of a soft ferromagnetic medium with a crack-like flaw. Fatigue & Fracture of Engineering Materials & Structures 26, 1091–1102.

Yang, W., Pan, H., Zheng, D., Cai, Q., 1999. An energy method for analyzing magnetoelastic buckling and bending of ferromagnetic plates in static magnetic fields. ASME Journal of Applied Mechanics 66, 913–917.

Zhou, Y.H., Miya, K., 1999. A theoretical prediction of increase of natural frequency to ferromagnetic plates under in-plane magnetic fields. Journal of Sound and Vibration 222, 49–64.

Zhou, Y.H., Zheng, X.J., 1996. A theoretical model of magnetoelastic buckling for soft ferromagnetic thin plates. Acta Mechanica Sinica 12, 213–224.